

# CrystEngComm

Accepted Manuscript



This is an *Accepted Manuscript*, which has been through the Royal Society of Chemistry peer review process and has been accepted for publication.

*Accepted Manuscripts* are published online shortly after acceptance, before technical editing, formatting and proof reading. Using this free service, authors can make their results available to the community, in citable form, before we publish the edited article. We will replace this *Accepted Manuscript* with the edited and formatted *Advance Article* as soon as it is available.

You can find more information about *Accepted Manuscripts* in the [Information for Authors](#).

Please note that technical editing may introduce minor changes to the text and/or graphics, which may alter content. The journal's standard [Terms & Conditions](#) and the [Ethical guidelines](#) still apply. In no event shall the Royal Society of Chemistry be held responsible for any errors or omissions in this *Accepted Manuscript* or any consequences arising from the use of any information it contains.

# Formation of Organic Molecular Nanocrystals under Soft Confinement

Xiaochuan Yang<sup>1</sup>, Ta-Chung Ong<sup>2</sup>, Vladimir K. Michaelis<sup>2</sup>, Scott Heng<sup>1</sup>, Robert G. Griffin<sup>2</sup> and Allan S. Myerson<sup>1,\*</sup>

<sup>1</sup> Novartis-MIT Center for Continuous Manufacturing and Department of Chemical Engineering, Massachusetts Institute of Technology, 77 Massachusetts Avenue, Cambridge, MA 02139, USA

<sup>2</sup> Department of Chemistry and Francis Bitter Magnet Laboratory, Massachusetts Institute of Technology, 77 Massachusetts Avenue, Cambridge, MA 02139, USA

**KEYWORDS:** orally dissolving films, poorly soluble APIs, organic molecular nanocrystals, NMR, soft confinement.

---

**ABSTRACT:** Methods to produce nano-sized organic molecular crystals in thin films are of great interest in the pharmaceutical industry due to the potential benefit of increased solubility of poorly soluble drugs and the advantages of film-based dosage forms over traditional tablet/capsule-based dosage form. One method to directly form organic nanocrystals is by crystallization in confined environments where the overall crystallization volume is constrained. We report the use of a novel solution impregnation method to form nanocrystals in polymer matrices with various microstructures in order to study the structure of the confined nanocrystals and the role of soft confinement and polymer chemistry on the nucleation process of nano-sized crystals. The particle diameter correlates with the microstructure of the polymer matrices and the nucleation kinetics. In addition, by carefully choosing the experimental conditions and the polymer matrix, polymorph control of nanocrystals can be achieved. Solid-state nuclear magnetic resonance (ssNMR) was used to examine the local structure of nanocrystals inside the polymer matrices and crystal polymer interactions. This method may serve as a novel formulation method to obtain nanocrystals of poorly soluble active pharmaceutical ingredients (APIs) for pharmaceutical industry.

---

## 1. Introduction

In recent years, interest in organic molecular nanocrystals has increased dramatically particularly in the pharmaceutical industry. It is estimated that 40% or more of organic compounds identified through combinatorial screening exhibit poor aqueous solubility,<sup>1</sup> and formulating these compounds as nanocrystals may potentially increase their bioavailability.<sup>2</sup> As crystal size decreases, surface-to-volume (s/v) ratios greatly increase and thus the dissolution rate is strongly enhanced. In addition, as the Ostwald-Freundlich equation predicts, the solubility of nano-sized crystals smaller than 1  $\mu\text{m}$  is much higher than that of larger bulk crystals.<sup>3</sup> Kim *et al.* demonstrated a 31.7% solubility enhancement by formulating  $\beta$ -glycine as nanocrystals, of which the equivalent radius is 244 nm.<sup>4</sup> Wang *et al.* showed that carbamazepine form III nanocrystals with diameter of  $\sim 320$  nm exhibited a 26.4% increase in their solubility.<sup>4,5</sup> Methods to produce organic molecular nano-sized crystals have been widely studied. Based on the crystal formation process, methods to form nano-crystals can be divided into two categories: “top-down” and “bottom-up”. Top-down methods refer to those that break large crystals into smaller ones, such as milling and high pressure homogenization. However, the introduction of impurities, high-energy consumption, and possible polymorph transformation are major drawbacks of these approaches. Bottom-up methods refer to those that aggregate single molecules into nano-scale crystals, such as emulsification<sup>6,7</sup>, supercritical fluid crystallization<sup>8,9</sup>, impinging jet crystallization<sup>10,11</sup>, and confined crystallization. However, the high supersaturation and/or high inten-

sity mixing involved make control of crystal size and polymorphs difficult. Microfluidic devices can be used to produce nanocrystals with uniform size distribution, but these devices experience channel clogging, which negatively impacts the continuous mass production of crystals.<sup>12-14</sup>

Direct formulation of pharmaceutical nanocrystals in thin films has been considered a novel formulation approach in industry recently, along with advanced manufacturing technologies such as continuous manufacturing advocated by the US Food and Drug Administration and many leading pharmaceutical firms<sup>15,16</sup>. Nano-crystallization in many types of confinements has been reported in the literature including the use of rigid inorganic porous materials such as controlled pore glasses<sup>17-20</sup>, mesoporous silica<sup>21</sup> and zeolites<sup>22</sup>. Recently, the use of soft confinement materials such as porous polymers has become popular. Ward and coworkers reported using porous polystyrene-poly(dimethyl acrylamide) (p-PS-PDMA) monoliths to obtain nano-sized crystals of  $\beta$ -glycine, 2,2,3,3,4,4-hexafluoro-1,5-pentanediol and (R)-(+)-3-methyladipic acid.<sup>17,18</sup> Diaio *et al.* used polymer gels with tunable microstructures and polymer nano-pores of different shapes and angles to control nucleation kinetics and polymorphic outcomes.<sup>23-25</sup> Besides, from a pharmaceutical formulation perspective, polymer film based dosage forms possess certain advantages over conventional tablets or capsules. For example, orally dissolving film is a promising dosage form and it recently attracted more research efforts<sup>26</sup> because (i) it serves as an alternative for patients experiencing swallowing difficulties, (ii) it may be formulated through absorption in the mouth

(sublingually or buccally) to improve bioavailability and (iii) some direct formulation methods, like the one introduced in this work, do not require powder mixing of active pharmaceutical ingredients (APIs) and excipients. This may avoid issues associated with particle handling including poor particle flowability of API and excipient raw materials.

Despite these increased research efforts, understanding the structure of the confined nanocrystals and their respective crystalline-polymer interactions remain a challenge<sup>27</sup>. We present a novel bottom-up method to directly produce nanocrystals in thin-film polymer matrices with analysis by magic-angle spinning (MAS) nuclear magnetic resonance (NMR) to understand the nucleation kinetics and structures of organic molecular nanocrystals formed inside soft confined environments. The model polymer matrix is composed of cross-linked cellulose/cellulose acetate polymer fibers with various pore sizes. We propose that by varying the microstructures of these polymer matrices nano-sized crystals with controlled polymorphic outcome can be obtained and stabilized.

## 2. Experimental Section

**Materials:** Glycine (ReagentPlus<sup>®</sup>,  $\geq 99\%$ ), acetaminophen (BioXtra<sup>®</sup>,  $\geq 99.0\%$ ), ibuprofen ( $\geq 98\%$ ) and water (CHROMASOLV<sup>®</sup>, for HPLC) were purchased from Sigma Aldrich. Deferasirox was a gift from Novartis. Porous cellulose membranes (Whatman<sup>®</sup>, pore size 200/450/1000 nm, thickness 75  $\mu\text{m}$ ) and cellulose acetate membranes (Whatman<sup>®</sup>, pore size 200/450/800/1200 nm, thickness 140  $\mu\text{m}$ ) were purchased from GE Healthcare Life Sciences. Ethanol (200 proof) was purchased from VWR.

**X-Ray Powder Diffraction (XRPD) Analysis:** The instrument (X'Pert PRO, PANalytical Inc.) is equipped with a PW3050/60 standard resolution goniometer and a PW3373/10 Cu LFF DK241245 X-ray tube. The high tension generator high voltage and anode current were set at 45 kV and 40 mA. A spinner sample stage PW3064 (Reflection mode) was used for all samples. Settings on incident beam path include: soller slit 0.04 rad., mask fixed 10 mm, programmable divergence slit and fixed 1° anti-scatter slit. Settings on diffracted beam path include: soller slit 0.04 rad and programmable anti-scatter slit. The scan was programmed as a continuous scan: 2 $\theta$  angle 2–40°, step size 0.0083556°, time per step 19.685 s; three repeated scans were collected to average the signal.

**Differential Scanning Calorimetry (DSC) Analysis:** The instrument (Q2000, TA instruments) was maintained with nitrogen gas flow at a rate of 50 ml/min in order to create an inert gas environment in the sample chamber. An extra refrigerated cooling system (RCS 40, TA instruments) is used to extend the available temperature range between -40 and 400 °C. Tzero<sup>®</sup> pans and lids were used. A heating/cooling rate of 5°C/min was applied for all samples, and the initial and final temperatures were adjusted accordingly based on the melting points of the various organic compounds. For example, the temperature was adjusted between 20 and 80 °C for ibuprofen since its melting point is  $\sim 75$  °C.

**Solid-state Nuclear Magnetic Resonance:** Magic-angle spinning NMR experiments were conducted on a home-built 500 MHz spectrometer (courtesy of Dr. Dave Ruben, Francis Bitter Magnet Laboratory - MIT) using either a 3.2 mm or a 4 mm Varian triple resonance (<sup>1</sup>H/<sup>13</sup>C/<sup>15</sup>N) MAS probe. For the cross-polarization (CP) experiments,<sup>28</sup> the contact time was

optimal at 2 ms ( $\gamma B_1/2\pi = 83$  kHz). The spinning frequency was set between 10 and 13.5 kHz, while <sup>1</sup>H spin-lattice relaxation times,  $T_1$  were measured either by the inversion-recovery<sup>29</sup> or the saturation recovery<sup>30</sup> sequence. All experiments were acquired using high-power two pulse phase modulation (TPPM)<sup>31</sup> proton decoupling ( $\gamma B_1/2\pi = 83$  kHz). Recycle delays varied from 5 s (e.g., ibuprofen) to 120 s (e.g., acetaminophen) and up to 4,096 co-added transients were acquired. All <sup>13</sup>C MAS NMR spectra were referenced to 40.49 ppm using solid adamantane with respect to DSS (0 ppm). Quantification of API polymorphs from CPMAS spectra was performed following the procedure published by Offerdahl *et al.*<sup>32</sup>

**Scanning Electron Microscope (SEM) Imaging:** A JEOL<sup>®</sup> 6700F SEM (cold field-emission gun scanning electron microscope) was used to obtain SEM images. The matrix cross-section imaging by SEM is challenging since the polymer matrix is not conductive. Cryo-cutting techniques were applied to freeze the sample before cutting in order to maintain the micro-structures of the nanocrystals within the matrix: (1) samples were submerged in liquid nitrogen for  $\sim 30$  minutes; (2) samples were quickly transferred onto two wooden supports with a 5-mm gap in between, and the sample was easily cracked into two pieces when a tweezer tip was pressed onto the sample; (3) one piece was then coated with a  $\sim 20$  nm gold thin film for creating a conductive surface under the SEM; (4) the sample was attached onto a vertical support on a special aluminum SEM sample holder (Electron Microscopy Sciences, catalog 75344) with the cracked cross-sectioned part facing upwards. This approach was used due to concern that a large portion of nanocrystals near the cross-sectioned part may be lost due to cutting, unintentional shaking or sudden exposure to environmental humidity.

**Sample Preparation:** Nano Plotter (Model NP2.1, GeSim Germany) was used to uniformly disperse solution droplets onto a porous matrix. The instrument can disperse a desired number of droplets onto any desired spot by micromachined piezoelectric micropipettes. Based on the porosity and the affinity of the solution for the matrix, we experimented and designed programs in order to disperse solution droplets uniformly onto the matrix without residual solution on the surface. Key parameters that vary for different solutions include concentration, the number of droplets per spot and step size between spots. Nano Plotter also includes an enclosure in which an open beaker containing a solution of a certain concentration can be placed to control the relative vapor pressure. For example, raising the vapor pressure of ethanol may slow down the evaporation and crystallization of acetaminophen/ethanol solution, and thereby promoting the production of a more stable polymorphic crystalline form.

## 3. Results & Discussion

Glycine (GLY), ibuprofen (IBP), acetaminophen (APAP) and deferasirox (DFX) were selected as model compounds to represent active pharmaceutical ingredients exhibiting simple to complex structures (Figure 1a). GLY has a total of six different polymorphs; three forms ( $\alpha$ ,  $\beta$  and  $\gamma$ ) can be obtained under standard ambient temperature and pressure. IBP was reported as having two polymorphs (I and II), but the second polymorph was only successfully produced in a very small amount (milligrams) with a complicated heating and quenching loop<sup>33</sup>. APAP possesses three polymorphs (I, II and III):

form I is the most stable and commercially formulated form. DFX was reported to have five polymorphs (I-V), and the most stable form (polymorph I) is chosen in the marketed formulation.

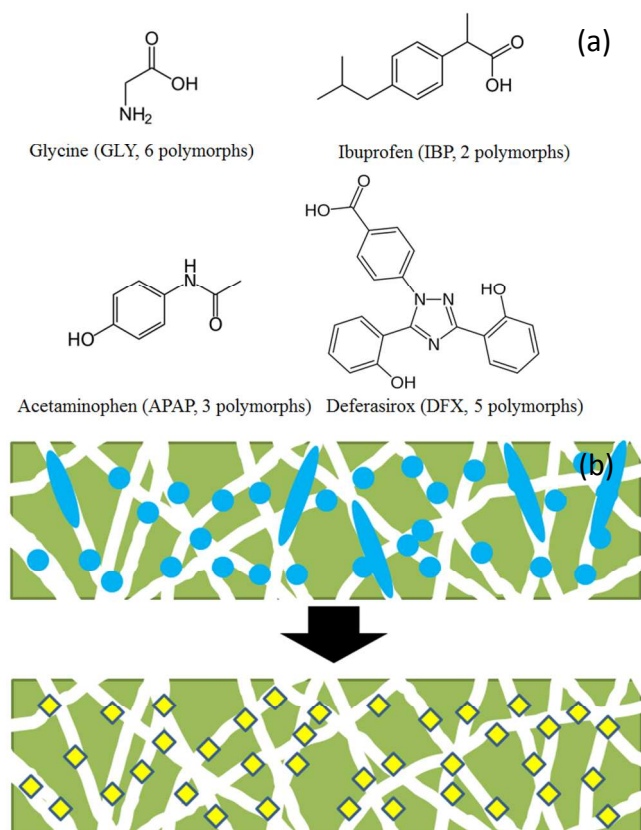


Figure 1. (a) Molecular structures for four relevant pharmaceutical targets as studied below. (b) Schematic illustration of the designed nano-crystallization process: use drop by demand techniques to disperse picoliter droplets into the membrane matrices and slowly evaporate the solution to form nanocrystals with good content uniformity.

### (i). Drug loading and method feasibility

The uniformity of nanocrystals distributed inside the porous matrix (directly related to content uniformity per dose) and minimizing the existence of surface crystals are vital for this technique as a practical formulation method (a schematic illustration is drawn as Figure 1b). The large surface crystals could serve as new nucleation sites when confined nanocrystals dissolve and impact the expected bioavailability. Several considerations regarding experimental parameters were taken into account in order to achieve the desired content uniformity as well as minimal number of surface crystals. First, the dispersed droplet size was minimized, so it would be easy for the droplets to infiltrate the matrix without significant volume of liquid suspended on the surface. As shown in Figure 2a and b, we obtained droplets dispersed from the Nano Plotter using three different solvents. The volume of droplets are  $\sim 77$ - $181$  pL (corresponding diameter  $\sim 43$ - $56$   $\mu\text{m}$ , which is the same order of magnitude as the membrane thickness, cellulose  $75$   $\mu\text{m}$  and cellulose acetate  $140$   $\mu\text{m}$ ). Second, the step size of dispersion was far enough to ensure the least interference of two adjacent droplets and yet close enough to achieve a relatively high drug loading if required by formulation needs. Fig-

ure 2c shows droplets of ethanol dispersed onto a glass slide surface, showing good uniformity of dispersion. By adjusting the equipment parameters, droplet volume and step size could be controlled for different solutions. For example, we made a solution of  $4$  g ibuprofen in  $10$  ml ethanol. A single droplet size was tuned to  $\sim 56$   $\mu\text{m}$  by diameter and the step size was set to  $50$   $\mu\text{m}$ . A cellulose membrane ( $200$  nm pore size) was cut into a square shape with each side being  $30$  mm in length and secured onto the Nano Plotter sample plate. After the dispersion was finished, we waited at least  $12$  hours for crystallization. The sample was placed into a vacuum oven overnight to evaporate all residual solvents, and no significant loss of mass was observed.

After crystallization, the membrane was inspected for surface crystals and recorded the mass increase due to API loading. Using a microscope (objective lens  $100\times$  and eyepiece lens  $10\times$ ), no surface crystals were observed. This is likely a result of the membranes exhibiting good affinity towards water and ethanol; therefore the solution diffused into the matrix very quickly and left little residue on the surface. Table 1 summarizes the loading results. They match well with the designed loading amounts, demonstrating that almost all droplets were successfully loaded and embedded into the polymer matrix. In other words, this drop-on-demand formulation approach showed good achievement regarding content weight, uniformity and delivery of solution into the porous films.

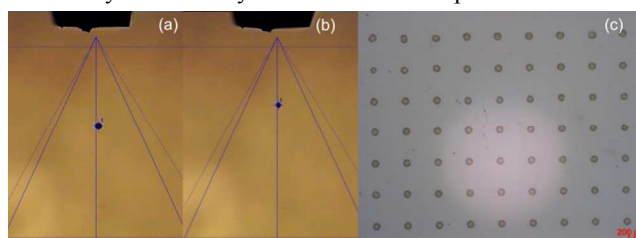


Figure 2. Inspection of droplets generated from the Nano Plotter. (a) Pure DMSO droplets generated by Nano Plotter. (b) Ibuprofen/ethanol droplets generated by Nano Plotter. The solvent was ibuprofen/ethanol solution and the droplet size is  $181$  pL. The diameter of the droplet is  $57$   $\mu\text{m}$ . (c) Array of glycine crystals (result of dispersing glycine/water solution droplets onto a glass slide). The inspection demonstrated that the droplets are very uniform in size and the dispersion process is stable.

**Table 1. Mass loadings of different APIs inside porous membranes (unit:  $\text{mg}/\text{cm}^2$ ).**

API	GLY	IBP	APAP	DFX
Mass	$9.8 \pm 0.4$	$23.1 \pm 0.6$	$8.4 \pm 0.3$	$5.8 \pm 0.4$

### (ii). Size analysis of nanocrystals inside the membrane pores

Preparing nanocrystals as small as possible is one of the goals of this work. However, characterizing nanocrystals inside a polymer matrix is challenging. Generally, organic compounds have a low melting point and can accumulate electrons under SEM. As mentioned in the experimental section, cryo-cutting was used to prepare cross-sectioned parts of samples. Figure 3 shows SEM images of a cross-sectioned part of a

membrane loaded with 23.0 wt% ibuprofen nanocrystals. Figure 3a clearly shows the cross-linked structure of cellulose fibers. Figure 3c is an enlarged image of a small part of Figure 3b. These images show that there was no micrometer scaled ibuprofen crystal in the membrane. Due to the high energy nature of SEM focus spot, these organic nanocrystals melted too quickly when we reached for even higher magnifications. Nevertheless, given the high mass loading and confirmation of fully crystalline materials via MAS NMR, it is reasonable to infer that the ibuprofen crystals must be in the nanometer range. We examined many other regions on the cross sectioned sample of the membrane under SEM, and did not find observable difference between regions in the middle and regions near the surface of the membrane. X-ray diffraction (peak width) could be utilized as a method to estimate the size of the formed nanocrystals. However, it can only be used to provide a rough estimate because many other factors such as crystal defects and structure deformation (micro strain) may also contribute to the peak broadening, and preferred orientation effect will also change the peak height and alter the peak shape.

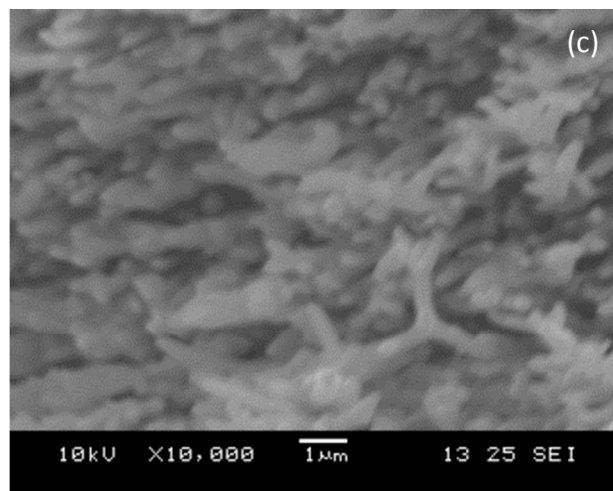
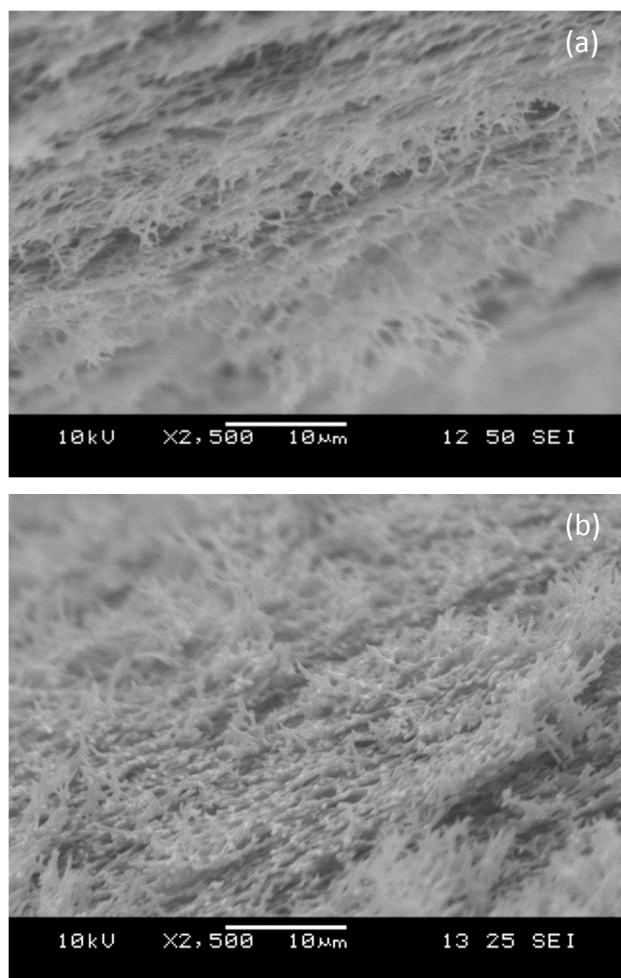


Figure 3. SEM images of a cross-sectioned part of a cellulose membrane (200 nm pores, a), a cross-sectioned part of a cellulose membrane loaded with ibuprofen nanocrystals (200 nm pores, b), and a zoomed image of (b) with a scale bar of 1  $\mu\text{m}$  (c). The loading fraction is 23.0 wt. %. The membrane consists of cross-linked cellulose polymer fibers.

### (iii). Effect of pore sizes

The size of confinement plays a significant role in nucleation kinetics and influences the polymorphic outcomes. Previous literature focused on small confinements from  $< 1$  nm to  $\sim 50$  nm, and result in amorphous materials if supersaturation generation is not controlled well.<sup>17-19, 24, 34-36</sup> In this work we initially attempted several polymer matrices with pore sizes ranging 10 - 40 nm. However, with ibuprofen, these pore sizes produced amorphous material even with very slow evaporation over a period of one week. Considering the potential industrial application, we instead use the commercially available cellulose membrane with pore sizes of approximately 200 to 1,000 nm. Table 2 and 3 summarize the results, showing the polymorphic outcomes of various crystals in membranes that have pore sizes  $\geq 200$  nm. The GLY experiments were performed with a relative humidity control (75%RH). Other experiments were operated at ambient conditions without controlling the solvent vapor pressure since some parts of the equipment are sensitive to organic solvents. As pore size decreased, GLY crystallized as the  $\beta$ -form and APAP partially produced the metastable form II. Using  $^{13}\text{C}$  CP MAS NMR it was confirmed that no detectable amount of amorphous materials was produced.

**Table 2 polymorphic outcome of compounds crystallized in cellulose membranes of different pore sizes.**

Pore Size (nm)	GLY	IBP	APAP	DFX
200	$\beta$	I	I,II	I
450	$\alpha,\beta$	I	I	I
1,000	$\alpha,\beta$	I	I	I

**Table 3 polymorphic outcome of compounds crystallized in cellulose acetate membranes of different pore sizes.**

Pore Size (nm)	GLY	IBP	APAP	DFX
200	$\beta$	I	I,II	I
450	$\alpha,\beta$	I	I	I
800	$\alpha,\beta$	I	I	I
1,200	$\alpha$	I	I	I

We considered using XRPD to quantify the fraction of different polymorphs in the samples, but the preferred orientation and interference of cellulose/cellulose acetate background made this impossible. The preferred orientation effect from the (100) plane is prominent in the GLY XRPD, as shown in Figure 4. This is probably due to the carboxyl group ( $-\text{COOH}$ ) of glycine molecules forming hydrogen bonds with the hydroxyl groups ( $-\text{OH}$ ) of cellulose and therefore glycine mainly crystallized along the (100) plane, as shown in Figure 5.

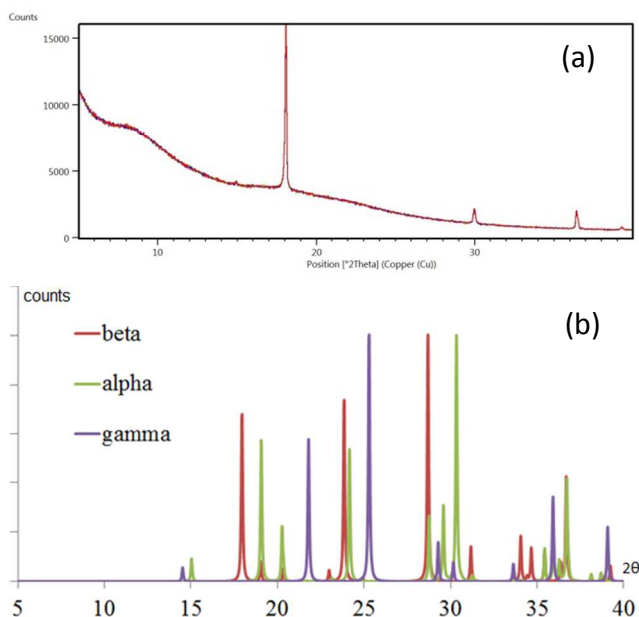


Figure 4. XRPD pattern of  $\beta$ -glycine in a cellulose membrane of 200 nm pore size (a) and calculated patterns of different polymorphs of glycine (b). The very intense peak ( $2\theta \approx 18^\circ$ ) in (a) corresponding to the (100) plane of  $\beta$ -glycine.

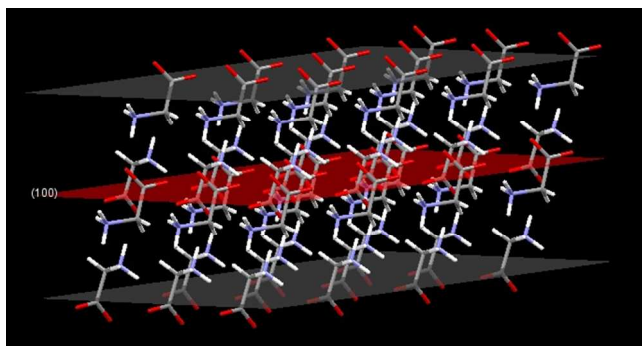


Figure 5. Crystal structure of  $\beta$ -glycine on the surface of cellulose fibers, the carboxyl group of the glycine molecules may form

hydrogen bonds or interact strongly with the hydroxyl groups of the cellulose membrane and cause the preferred orientation to be the (100) plane.

#### (iv). Melting point depression

The Gibbs-Thomson equation (Eqn. 1) is widely used to explain the melting point reduction as a function of particle size. As the particle size reduces, the melting point of the particle also decreases.  $T(d)$  is the melting temperature,  $d$  is the particle size in diameter,  $T_{bulk}$  is the melting point of bulk crystal,  $\sigma_{sl}$  is the crystal-melt interfacial energy,  $H_f$  is the crystal molar heat of fusion, and  $\rho_s$  is crystal density:

$$T(d) = T_{bulk} \left( 1 - \frac{4\sigma_{sl}}{H_f \rho_s d} \right) \quad (1)$$

Table 4 shows the DSC results of ibuprofen nanocrystallized in various membranes. Each data point was averaged from at least three different samples. By assuming the size of the nanocrystals to be the same as the pore sizes, we found there is a linear relationship between the melting point and the crystal size, although the errors bars are significant compared to the effect.

**Table 4 Melting points of ibuprofen in various membranes**

Cellulose pore (nm)	Melting point ( $^\circ\text{C}$ )	Cellulose acetate pore (nm)	Melting point ( $^\circ\text{C}$ )
200	$74.0 \pm 0.3$	200	$73.2 \pm 0.1$
450	$74.5 \pm 0.2$	450	$74.3 \pm 0.2$
1000	$74.8 \pm 0.2$	800	$74.6 \pm 0.2$
		1200	$75.0 \pm 0.1$

\* Bulk ibuprofen  $75.1 \pm 0.1$   $^\circ\text{C}$

We likewise noticed that different polymer matrices also contributed to observed melting point depressions. For the same pore size, the melting point of IBP crystallized in cellulose acetate was depressed by  $0.8$   $^\circ\text{C}$  relative to those in cellulose, as shown in Figure 6. This is probably explained by the interactions of IBP molecule with the membrane surface. Cellulose has hydroxyl ( $-\text{OH}$ ) groups that may interact with the carboxylic acid ( $-\text{COOH}$ ) group of ibuprofen. This preferred interaction may promote nucleation kinetics, and therefore crystals will grow quickly and larger than the crystals in cellulose acetate membranes.

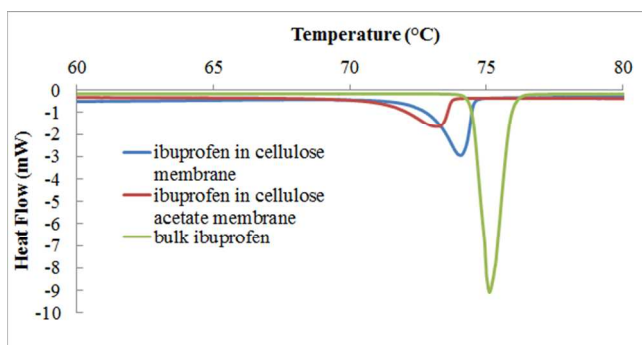


Figure 6. DSC analysis of three samples: ibuprofen nanocrystals loaded in cellulose membrane of 200 nm pores (blue,  $73.2 \pm 0.1$  °C), ibuprofen nanocrystals loaded in cellulose acetate membrane of 200 nm pores (red,  $74.0 \pm 0.3$  °C) and bulk ibuprofen crystals directly from a commercial source (green,  $75.1 \pm 0.1$  °C).

#### (v). Structure information analyzed by MAS NMR

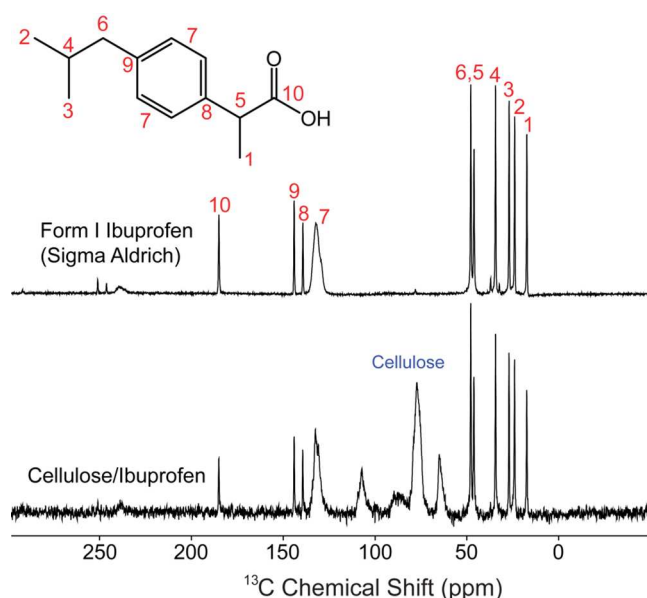


Figure 7.  $^{13}\text{C}$  CP MAS NMR spectra of form I ibuprofen (top) and cellulose-ibuprofen (bottom) acquired at 11.7 T (500 MHz,  $^1\text{H}$ ). The cellulose resonance is located between the ibuprofen aliphatic and aromatic carbon ( $> 50$  and  $< 140$  ppm) resonances, and no spectral overlap occurs.

Table 5.  $T_1$  ( $^1\text{H}$ ) of form I ibuprofen and cellulose-ibuprofen

Chemical Shift	$T_1$ ( $^1\text{H}$ ) (s)	$T_1$ ( $^1\text{H}$ ) (s)
( $\delta_{\text{iso}}$ , ppm)	Form I Ibuprofen	Cellulose-Ibuprofen
185.0	$1.18 \pm 0.08$	$1.14 \pm 0.11$
144.1	$1.21 \pm 0.05$	$1.15 \pm 0.09$
139.3	$1.19 \pm 0.06$	$1.08 \pm 0.10$
47.9	$1.22 \pm 0.02$	$1.25 \pm 0.05$

46.1	$1.21 \pm 0.03$	$1.27 \pm 0.04$
34.4	$1.17 \pm 0.03$	$1.19 \pm 0.06$
27.0	$1.13 \pm 0.05$	$0.87 \pm 0.06$
24.0	$1.10 \pm 0.06$	$0.81 \pm 0.05$
17.3	$1.11 \pm 0.06$	$0.83 \pm 0.06$

We compared the assigned CP MAS NMR spectra of form I crystalline IBP, the stable polymorph as obtained from Sigma Aldrich, and of cellulose-ibuprofen as shown in Figure 7. The form I IBP exhibits sharp resonances with a linewidth (full-width at half maximum) of 54 Hz, or 0.4 ppm, which is consistent with literature.<sup>37,38</sup> Upon incorporation of IBP into the cellulose membrane (200 nm pore size), we found that the resonances of cellulose-ibuprofen share the same  $^{13}\text{C}$  isotropic chemical shifts and linewidths as the form I IBP. This finding therefore suggests that IBP exists entirely as form I within the pores of the cellulose membrane, and no additional polymorph was formed. A comparison of  $^1\text{H}$  spin-lattice relaxation time constants ( $T_1$ ) of form I and cellulose-ibuprofen revealed similar  $T_1$  values within experimental error (Table 5), which is further evidence that the cellulose excipient seemingly does not perturb the structure and the dynamics of IBP.

In contrast with IBP, APAP polymorphism was readily observed within the cellulose membrane. Compared to the  $^{13}\text{C}$  CP MAS NMR spectrum of the stable monoclinic form I APAP, the spectrum for the cellulose-acetaminophen shows resonance peak splitting that indicates a mixture of polymorphs are formed inside the membrane pores, as shown in Figure 8. The difference in isotropic chemical shifts between the polymorphs is not large, but distinct resonances are resolvable for a few  $^{13}\text{C}$  sites as shown in Figure 9. The  $^{13}\text{C}$  isotropic chemical shifts of these additional resonances are consistent with the data published by Moynihan and O'Hare<sup>39</sup> for the orthorhombic form II acetaminophen. The ratio of form I and the form II acetaminophen within the cellulose membrane is 65:35.

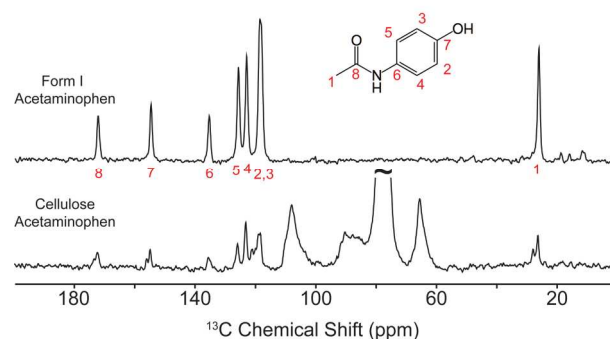


Figure 8.  $^{13}\text{C}$  CP MAS NMR spectra of form I acetaminophen (top) and cellulose-acetaminophen (bottom).

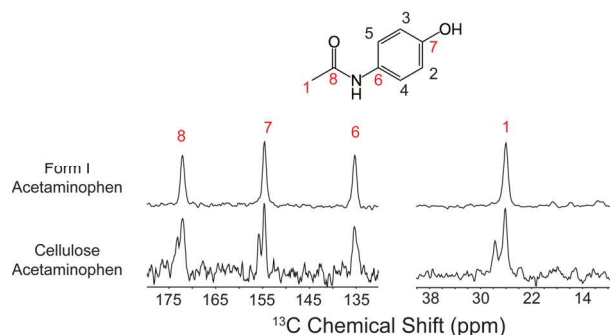


Figure 9. Expanded  $^{13}\text{C}$  CP MAS NMR spectra of acetaminophen of the  $^{13}\text{C}$  resonances sensitive to polymorphism clearly illustrate the onset of form II observed in the cellulose-acetaminophen formulation.

In addition to the onset of polymorphs, a notable difference between form I acetaminophen and the cellulose-acetaminophen is the measured  $^1\text{H}$   $T_1$ . The crystalline form I acetaminophen has  $^1\text{H}$   $T_1$  that is longer than 100 s, but once inside the membrane acetaminophen  $T_1$  reduces to less than 20 s, as summarized in Table 6. This finding is evidence that no bulk microcrystalline acetaminophen was formed on the membrane surface, because the reduction of  $^1\text{H}$   $T_1$  can be attributed to spin diffusion through the cellulose membrane, which has  $^1\text{H}$   $T_1$  of approximately 6 s. Possible factors such as structural disorder and/or crystal defects can also serve as relaxation sinks that reduce acetaminophen  $T_1$  within the membrane.

Table 6.  $T_1$  ( $^1\text{H}$ ) of form I acetaminophen and cellulose-acetaminophen.

Chemical Shift ( $\delta_{\text{iso}}$ , ppm)	$T_1$ ( $^1\text{H}$ ) (s) Form I Acetaminophen	$T_1$ ( $^1\text{H}$ ) (s) Cellulose-Acetaminophen
171.8	127 $\pm$ 15	18.5 $\pm$ 1.3
154.3	122 $\pm$ 13	19.0 $\pm$ 1.0
135.0	129 $\pm$ 15	17.3 $\pm$ 1.7
125.3	116 $\pm$ 13	16.6 $\pm$ 1.2
122.6	109 $\pm$ 11	18.7 $\pm$ 1.9
118.3	111 $\pm$ 14	17.3 $\pm$ 1.0
117.7	105 $\pm$ 9	19.9 $\pm$ 1.0
25.7	126 $\pm$ 16	17.8 $\pm$ 0.7

#### (vi) Dissolution enhancement and potential use in industry

In order to compare dissolution profiles of nanocrystals in membranes of different pore sizes, we chose IBP as the model

compound since it shows consistently the form I polymorph without detectable structure deformation in all the analysis shown above. The same amounts of IBP ( $20.8 \pm 0.6$  mg) were successfully loaded into cellulose membranes with 200, 450, and 1000 nm pores. For comparison, we also chose a control group that is a mixture of ibuprofen crystals from a commercial source (Sigma Aldrich) and membranes of 200 nm pores. The dissolution tests were conducted under the instruction of U.S. Pharmacopeia standards. Figure 10 illustrates the enhanced dissolution profiles of nanocrystals inside membranes. As shown in the figure, membranes of 200 nm pores showed the fastest release, and released twice as much IBP as the control group in one minute. The control group reached 80% release within 15 minutes, but it only took ~ 5, 7 and 12 minutes for membranes of 200, 450 and 1000 nm pores to achieve 80% release, respectively. The improvement in dissolution profiles is believed to be a combination effect of increasing the surface/volume ratio and improving solubility due to the reduction of crystal size (*vide supra*). There is a possibility that diffusion of the compound out of the polymer matrix into the bulk dissolution medium may play a role in limiting the whole release process, even though we already chose a relatively thin membrane (75  $\mu\text{m}$ ). From the perspective of polymer compositions, several alternatives may be possible: (a) rather than cellulose, we could use water-soluble polymers (*e.g.*, chitosan, etc.) as the base of the matrix. These polymers can dissolve quickly in water, but are insoluble to some organic solvents that can dissolve the desired API loading compounds; (b) some disintegrants could be blended into the matrix during the manufacturing process, so it will disintegrate into small pieces when coming in contact with water.

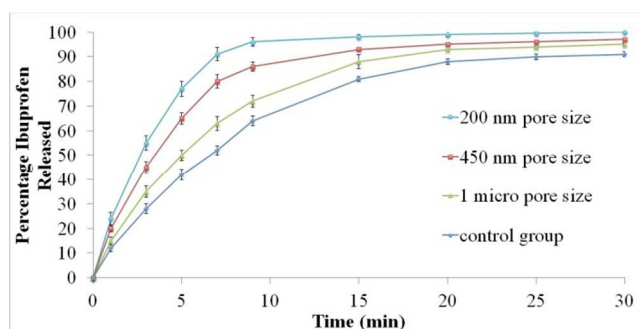


Figure 10. Dissolution test of cellulose membranes of different pore sizes loaded with the same mass of ibuprofen nanocrystals. The control group is ibuprofen crystals from commercial bottles (with a mean size of 48  $\mu\text{m}$ ) mixed with cellulose membranes of 200 nm pores. Each curve is averaged from at least three dissolution tests. Lines are guides for the reader.

#### 4. Conclusion

We demonstrate that the impregnation method using thin film polymer matrices is a promising mean to produce nano-sized organic molecular crystals with controlled polymorphs. This method provides several benefits: (1) The nanocrystals are directly embedded in the excipients, thereby avoiding transport problems of fine particles; (2) the drop-on-demand technique gives good controls on content loading amounts and uniformity; (3) crystal size and polymorphic outcome can be mastered by the pore size and surface chemistry of the polymer matrix; (4) polymer matrices may help block environmen-

tal humidity, separate nanocrystals in distances and confine them in certain dimensions to stabilize nanocrystals for a longer shelf life; (5) furthermore, the soft confinement (polymer matrices) may be a certain type of polymer or by addition of disintegrants that allow the matrices to immediately dissolve when coming into contact with water or from pH changes, like orally dissolving films. These results herein successfully demonstrate a promising formulation approach, and help advance the understanding towards crystallization behaviors of organic molecules in confined environments. This work has immense potential for industrial applications, and efforts are underway to further develop this technique.

## AUTHOR INFORMATION

### Corresponding Author

\* myerson@mit.edu

## ACKNOWLEDGMENT

We thank the Novartis-MIT Continuous Manufacturing Center for the continuous funding of the research presented here. NMR research at FBML-MIT is supported by the National Institutes of Health (NIH grant no. EB-002026). V.K.M. acknowledges the Natural Sciences and Engineering Research Council of Canada (NSERC) and the Government of Canada for a Banting Postdoctoral Fellowship.

## REFERENCES

1. E. M. Merisko-Liversidge and G. G. Liversidge, *Toxicologic pathology*, 2008, **36**, 43-48.
2. K. Kim, A. Centrone, T. A. Hatton and A. S. Myerson, *Crystengcomm*, 2011, **13**, 1127-1131.
3. W. Oswald, *Z. Phys. Chem*, 1900, **34**, 495-503.
4. K. Kim, I. S. Lee, A. Centrone, T. A. Hatton and A. S. Myerson, *Journal of the American Chemical Society*, 2009, **131**, 18212-+.
5. M. Wang, G. C. Rutledge, A. S. Myerson and B. L. Trout, *Journal of pharmaceutical sciences*, 2012, **101**, 1178-1188.
6. E. Kwon, H. Oikawa, H. Kasai and H. Nakanishi, *Crystal Growth & Design*, 2007, **7**, 600-602.
7. S. Petersen and J. Ulrich, *Chem Eng Technol*, 2013, **36**, 398-402.
8. M. Turk and R. Lietzow, *Journal of Supercritical Fluids*, 2008, **45**, 346-355.
9. E. Reverchon, G. D. Porta and M. G. Falivene, *Journal of Supercritical Fluids*, 2000, **17**, 239-248.
10. S. W. Siddiqui, Y. Zhao, A. Kukukova and S. M. Kresta, *Ind. Eng. Chem. Res.*, 2009, **48**, 7945-7958.
11. H. Chioua, H. K. Chana, D. Henga, R. K. Prudhomme and J. A. Raperc, *Journal of Aerosol Science*, 2008, **39**, 500-509.
12. M. Sultana, *Thesis: Microfluidic Systems for Continuous Crystallization of small organic molecules*, Massachusetts Institute of Technology, Cambridge, 2010.
13. V. Genota, S. Desportesb, C. Croushorea, J. Lefevrea, R. B. Pansua, J. A. Delairea and P. R. Rohrb, *Chemical Engineering Journal*, 2010, **161**, 234-239.
14. M. Ildefonso, N. Candoni and S. Veessler, *Crystal Growth & Design*, 2013, **13**, 2107-2110.
15. R. P. Dixit and S. P. Puthli, *Journal of Controlled Release*, 2009, **139**, 94-107.
16. S. Lee, T. O'Connor, X. Yang, C. Cruz, S. Chatterjee, R. Madurawe, C. V. Moore, L. Yu and J. Woodcock, *J Pharm Innov*, 2015, 1-9.
17. B. D. Hamilton, M. A. Hillmyer and M. D. Ward, *Crystal Growth & Design*, 2008, **8**, 3368-3375.
18. J.-M. Ha, M. A. Hillmyer and M. D. Ward, *The Journal of Physical Chemistry B*, 2005, **109**, 1392-1399.
19. J.-M. Ha, B. D. Hamilton, M. A. Hillmyer and M. D. Ward, *Crystal Growth & Design*, 2012, **12**, 4494-4504.
20. G. T. Rengarajan, D. Enke, M. Steinhart and M. Beiner, *Journal of Materials Chemistry*, 2008, **18**, 2537-2539.
21. K. K. Qian and R. H. Bogner, *Journal of pharmaceutical sciences*, 2012, **101**, 444-463.
22. P. Maheshwari, D. Dutta, S. K. Sharma, K. Sudarshan, P. K. Pujari, M. Majumder, B. Pahari, B. Bandyopadhyay, K. Ghoshray and A. Ghoshray, *The Journal of Physical Chemistry C*, 2010, **114**, 4966-4972.
23. Y. Diao, M. E. Helgeson, A. S. Myerson, T. A. Hatton, P. S. Doyle and B. L. Trout, *Journal of the American Chemical Society*, 2011, **133**, 3756-3759.
24. Y. Diao, M. E. Helgeson, Z. A. Siam, P. S. Doyle, A. S. Myerson, T. A. Hatton and B. L. Trout, *Crystal Growth & Design*, 2011, **12**, 508-517.
25. V. López-Mejías, A. S. Myerson and B. L. Trout, *Crystal Growth & Design*, 2013, **13**, 3835-3841.
26. M. N. Siddiqui, G. Garg and P. K. Sharma, *Advances in Biological Research*, 2011, **5**, 291-303.
27. C. Brough and R. O. Williams Iii, *International Journal of Pharmaceutics*, 2013, **453**, 157-166.
28. A. Pines, J. S. Waugh and M. G. Gibby, *J Chem Phys*, 1972, **56**, 1776-1777.
29. R. L. Vold, J. S. Waugh, M. P. Klein and D. E. Phelps, *J Chem Phys*, 1968, **48**, 3831-3832.
30. R. Freeman and H. D. W. Hill, *J Chem Phys*, 1971, **54**, 3367-3377.
31. A. E. Bennett, C. M. Rienstra, M. Auger, K. V. Lakshmi and R. G. Griffin, *J Chem Phys*, 1995, **103**, 6951-6958.
32. T. J. Offerdahl, J. S. Salsbury, Z. D. Dong, D. J. W. Grant, S. A. Schroeder, I. Prakash, E. M. Gorman, D. H. Barich and E. J. Munson, *J Pharm Sci-Us*, 2005, **94**, 2591-2605.
33. P. Derollez, E. Dudognon, F. Affouard, F. Danede, N. T. Correia and M. Descamps, *Acta Crystallographica Section B*, 2010, **66**, 76-80.
34. J. M. Ha, J. H. Wolf, M. A. Hillmyer and M. D. Ward, *J. Am. Chem. Soc.*, 2004, **126**, 3382.
35. Y. Diao, M. E. Helgeson, A. S. Myerson, T. A. Hatton, P. S. Doyle and B. L. Trout, *J. Am. Chem. Soc.*, 2011, **133**, 3756.
36. Y. Diao, T. Harada, A. S. Myerson, T. A. Hatton and B. L. Trout, *Nat. Mater.*, 2011, **10**, 867.
37. M. Geppi, S. Guccione, G. Mollica, R. Pignatello and C. A. Veracini, *Pharm Res*, 2005, **22**, 1544-1555.
38. J. P. Bradley, The University of Warwick, 2011.
39. H. A. Moynihan and I. P. O'Hare, *International Journal of Pharmaceutics*, 2002, **247**, 179-185.

TOC graph:

